Control Mechanisms for Gas Hydrate Production by Depressurization in Different Scale Hydrate Reservoirs

Liang-Guang Tang, Xiao-Sen Li,* Zi-Ping Feng, Gang Li, and Shuan-Shi Fan

Guangzhou Research Center for Gas Hydrate, Guangzhou Institute of Energy Conversion, The Chinese Academy of Sciences, Guangzhou, 510640, P. R. China

Received April 27, 2006. Revised Manuscript Received October 17, 2006

The methane hydrate was formed in a pressure vessel 38 mm in id and 500 mm in length. Experimental works on gas production from the hydrate-bearing core by depressurization to 0.1, 0.93, and 1.93 MPa have been carried out. The hydrate reservoir simulator TOUGH-Fx/Hydrate was used to simulate the experimental gas production behavior, and the intrinsic hydration dissociation constant (K_0) fitted for the experimental data was on the order of 10^4 mol m^{-2} Pa^{-1} s^{-1}, which was one order lower than that of the bulk hydrate dissociation. The sensitivity analyses based on the simulator have been carried out, and the results suggested that the hydrate dissociation kinetics had a great effect on the gas production behavior for the laboratory-scale hydrate-bearing core. However for a field-scale hydrate reservoir, the flow ability dominated the gas production behavior and the effect of hydrate dissociation kinetics on the gas production behavior could be neglected.

Introduction

Natural gas hydrates (NGHs) are crystalline, icelike compounds of natural gas and water molecules that are formed under certain thermodynamic conditions. These chemical compounds have natural-gas molecules included inside the cavities of icelike structure made by the water molecules through physical rather than chemical bonds.[1]

NGHs are treated as a potential energy resource for the 21st century because a large amount of methane gas is trapped in hydrate reservoirs both onshore buried under the permafrost and offshore buried under the oceanic and deep lake sediments.[2] Therefore, developing methods for commercial production of natural gas from hydrate reservoirs is attracting considerable attention. The suggested schemes of decomposition of hydrates include (1) thermal stimulation, to increase the system temperature above the temperature of hydrate formation at a specified pressure; (2) depressurization, to decrease the system pressure below the pressure of hydrate formation at a specified temperature; (3) chemical injection, to inject inhibitors such as methanol to shift the pressure−temperature equilibrium. The other two recent ideas which need experimental and field confirmation include: CO_2 replacement, to inject liquid CO_2 into offshore hydrate reservoirs by forming CO_2 hydrate and replacing the methane gas,[3] and gas lift, to lift the hydrate particle as a solid from the sea bottom.[4] However, among the various methods, the thermal stimulation combined with depressurization is regarded as the most promising mode for gas hydrate production.[5]

At the current stage when large-scale commercial hydrate production is impossible, the numerical simulation of a gas hydrate reservoir turns out to be a useful tool in predicting the dynamic properties of a gas hydrate reservoir undergoing different production modes. Several numerical models have been proposed for gas production from hydrate reservoirs in the last two decades.[6−10]

Yousif et al.[6] studied the hydrate dissociation kinetics in porous media with a one-dimensional (1D) isothermal model. In the model, the hydrate dissociation process was assumed to be isothermal. Gas and water flow were all considered in separated continuity equations, and the pressure of the gas and water was connected by capillary pressure. Variations of gas-phase permeability and porosity during the hydrate dissociation were also considered. The modeling results agreed well with their experimental data.

Masuda et al.[7] developed a 3D hydrate reservoir simulator. In this model, water and gas flow, conduction and convection heat transfer, and hydrate dissociation kinetics have been considered. The permeability reduction with hydrate saturation is also being modeled. Their numerical results were in agreement with their experimental data.

Ji et al.[8] developed a 1D analytical model for gas production from hydrate deposits. The thermal effect was considered while the hydrate kinetics and mobility of the water phase were ignored in this model. A set of self-similar solutions for

* Corresponding author. Phone: (8620)87057037. Fax: (8620)87057037. E-mail: lixs@ms.giec.ac.cn.

(1) Sloan, E. D. *Clathrate Hydrates of Natural Gas*, 2nd ed.; Marcel Dekker Inc: New York, 1998.

(2) Klauda, J. B.; Sandler, S. I. *Energy Fuels* **2005**, *19*, 459−470.

(3) Hirohama, S.; Shimoyama, Y.; Wakabayashi, A. *J. Chem. Eng. Jpn.* **1996**, *29*, 1014−1020.

(4) Hamaguchi, R.; Nishimura, Y.; Matsukuma, Y.; Minemoto, M. In *A Fluid Dynamic Study on Recovery System of Methane Hydrate*, Proceedings of the 5th International Conference on Gas Hydrate, Trondheim, Norway, June 12−16, 2005.

(5) Makogon, Y. F. *Hydrates of Natural Gas*, 1st ed.; Penn Well Publishing Company: Tulsa, OK, 1997.

(6) Yousif, M. H.; Abass, H. H.; Selim, M. S.; Sloan, E. D. *SPE Reservoir Eng.* **1991**, 69−76.

(7) Masuda, Y.; Fujinaga, Y.; Naganawa, S.; Fujita, K.; Sato, K.; Hayashi, Y. In *Modeling and Experimental Studies on Dissociation of Methane Gas Hydrates in Berea Sandstone Cores*, Proceedings of the 3rd International Conference on Gas Hydrates, Salt Lake City, USA, June 18−22, 1999.

(8) Ji, C.; Ahmadi, G.; Smith, D. H. *Energy Convers. Manage.* **2003**, *44*, 2403−2423.

(9) Moridis, G. J.; Collett, T. S. *J. Pet. Technol.* **2004**, *43*, 175−183.

(10) Moridis, G. J.; Kowalsky, M. B.; Pruess, K. *TOUGH-Fx/HYDRATE v1.0.1 User's Manual: A Code for the Simulation of System Behavior in Hydrate-Bearing Geological Media*; Lawrence Berkeley National Laboratory: Berkeley, CA, 2005; LBNL/PUB 3185.

10.1021/ef0601869 CCC: $37.00
Published on Web 12/08/2006

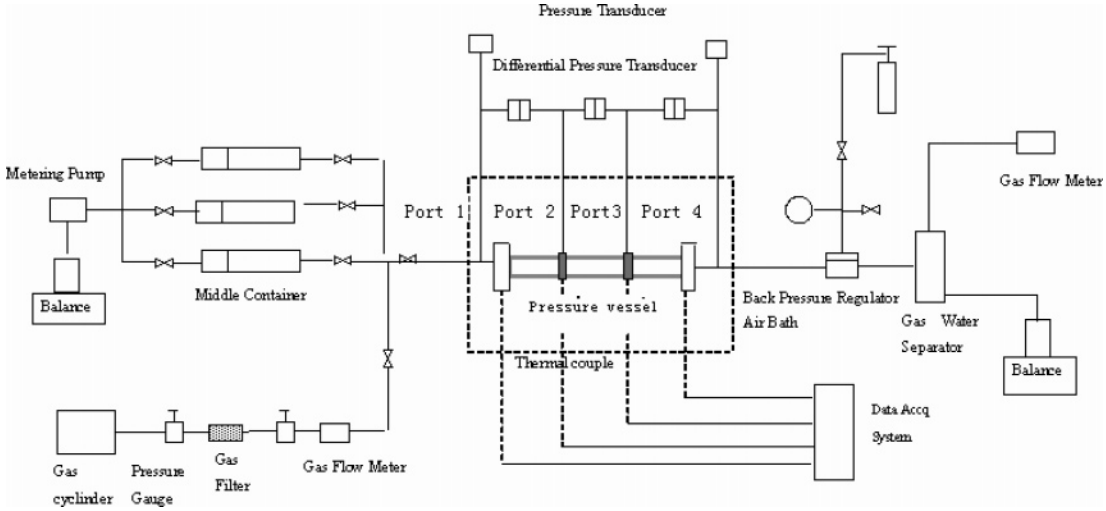

Figure 1. Schematic plot of the experimental facility.

temperature and pressure was obtained after linearization of the governing equations.

In 1998, Moridis[9] added a hydrate dissociation submodel, i.e., EOSHYDR, into TOUGH2, a general-purpose reservoir simulator, to simulate the behavior of a hydrate-bearing geological system. On the basis of the insights provide by this model, he developed a new code named TOUGH-Fx/Hydrate in 2005,[10] which could be the most comprehensive model in simulating gas hydrate production so far. By solving the coupled equations of mass and heat balance, it can model nonisothermal gas release, phase behavior, and flow of fluid and heat under conditions typical of common NGHs in complex geological media at any scale, from laboratory hydrate core to a field reservoir where Darcy's law is valid. The model includes both an equilibrium and kinetic model for hydrate formation and dissociation, and it accounts for heat and up to four mass components, i.e., water, CH_4, hydrate, and water-soluble inhibitors. The details can be found elsewhere.[10]

It should be pointed out that the system of hydrate dissociation is a complex system in which heat and mass transfer interact with hydrate kinetics. The developed simulator is helpful in encouraging a fundamental understanding of these systems, and the controlling regimes (flow, heat transfer, or kinetic) of the hydrate production processes can be identified through sensitivity analyses. However, for all the simulators, the hydrate intrinsic dissociation constant used is taken as the data from bulk hydrate dissociation without considering heat and mass transfer effects. An approach to develop the hydrate intrinsic dissociation constant in porous media from experimental works is necessary. Furthermore, in a recent study, Hong[11] stated that, among the three mechanisms, heat transfer and fluid flow had a large role in controlling gas production from hydrate, while hydrate dissociation kinetics became important only when the intrinsic rate constant was reduced by 5 orders of magnitude below the value found by Kim in a PVT cell,[12] which seems impractical from our recent simulation of hydrate dissociation experiments.

The main focus of this paper is to derive the hydrate intrinsic dissociation constant by fitting the laboratory hydrate depressurization experiments with the numerical simulation results from TOGUH-Fx/Hydrate and, then, to discuss the controlling mechanisms for different scale (laboratory- and field-scale) hydrate reservoirs during the production process.

Experiments

The schematic diagram of the experimental apparatus used in this work is shown in Figure 1. The pressure vessel as the main unit of the setup was immersed in an air bath with a temperature varying from −20 to 80 °C. The cell was made of stainless steel with internal diameter of 38 mm and length of 500 mm, and it can be operated up to 25 MPa. Four thermocouples and two pressure transducers with three differential pressure transducers were placed in four ports evenly along the vessel, as plotted in Figure 1, to measure the temperature and pressure profile along the vessel. A photograph of the pressure vessel is given in Figure 2.

The data acquisition unit recorded all the information varying with time, which included the pressure or differential pressure, temperature, gas/water injection rate, and gas/water production rate. In the cases using digital sensors and a data acquisition unit, the relationship between the measured values and real values has been established for the calibration. The pressure transducers, thermocouples, and mass flow meters were calibrated using a pressure test gauge with an error of ±0.05%, a mercury thermometer with a tolerance of ±0.01 °C, and a wet gas meter with an accuracy of ±10 mL/min, respectively.

During each experimental run, the raw dry sands were sieved into the size range of 300−450 μm and were pushed tightly into the vessel, resulting in the sediment with porosity around 33% and permeability of 300 mdarcy. The outlet valve was closed and the vessel was saturated with distilled water using a metering pump. Methane gas was then injected slowly at a pressure that is sufficiently higher than the equilibrium pressure at the working temperature. The amounts of injected distilled water and methane gas were recorded.

The vessel was then closed and kept at a steady environmental temperature for more than 8 h to be certain that there was no leakage of the system and that the gases dissolved into the water. After that, the temperature of the air bath was decreased to the working temperature. At the same time, the data acquisition system was started to acquire the data. Gas hydrates began to form in the vessel, and the hydrate formation was taken as finishing when there was no pressure decrease in the system, which lasted, in general, for 3−5 days. The formation process was repeated again after the hydrate was dissociated by increasing the environmental temperature to obtain homogeneous distributed hydrates in the system.

After the hydrate was formed at the second stage, the back pressure regulator was set to the experimental pressure, which is lower than the hydrate equilibrium pressure at the working temperature, and the outlet valve was opened quickly. The hydrate

(11) Hong, H.; Darvish, M. P. In *A Numerical Study on Gas Production from Formation Containing Gas Hydrates*, Proceedings of the Canadian International Petroleum Conference, Calgary, Alberta, Canada, June 10−12, 2003.

(12) Kim, H. C.; Bishnoi, P. R.; Heidemann, R. A.; Rizvi, S. S. H. *Chem. Eng. Sci.* **1987**, *42*, 1645−1653.

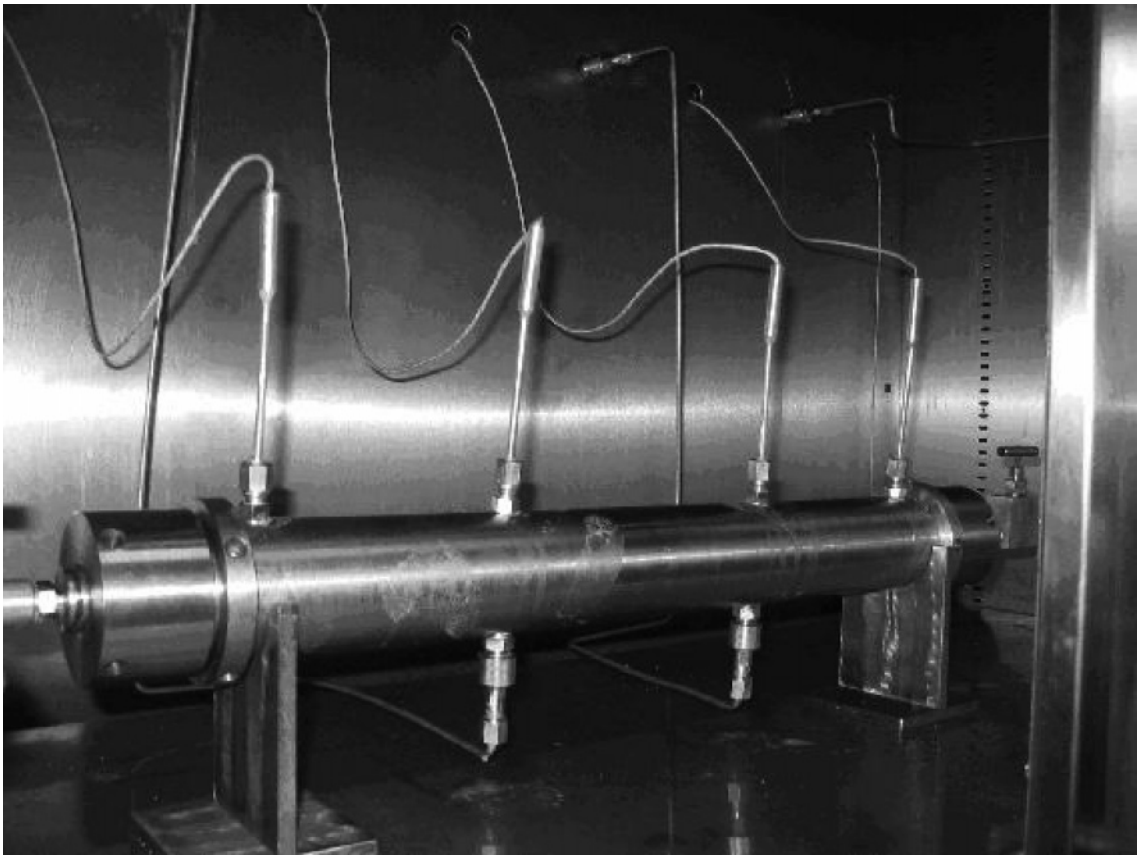

Figure 2. Photograph of the pressure vessel from the experimental facility.

Table 1. Experimental Condition for Hydrate Depressurization

run	1	2	3
initial pressure (MPa)	8.000	8.150	8.450
total injected gas (SCC[a])	10 744	10 809	12 562
total injected water (mL)	84.54	85.79	71.62
depressurization mode (MPa)	0.10	0.93	1.94
gas produced (SCC)	9758	8696	8280
water produced (mL)	34.70	47.09	48.80

[a] SCC stands for standard cubic centimeters.

began to dissociate. Gas and water were continuously released from the vessel through the outlet valve. When there was no significant gas released, the back pressure regulator was set at 0.1 MPa with the remaining gas released. The detailed experimental plan is given in Table 1.

Results and Discussion

1. Hydrate Formation. The inlet $P-T$ curve during the first stage hydrate formation and dissociation for a typical run is plotted in Figure 3. Due to the gas contraction upon cooling (A−B), the pressure decreases with temperature slowly, initially. A subcooling step (B−C) is needed for the hydrate formation after the gas + water + hydrate phase equilibrium $P-T$ reaches (B). The hydrate formation (C−D) can be observed in the figure when the pressure decreases sharply at a fixed temperature. The hydrate formation rate in porous media is slow, resulting in no temperature spikes in the curve. The hydrate begins to dissociate when the environmental temperature is raised until the pressure returns to the initial state (D−A). This kind of $P-T$ curve in general agrees with the result in the literature.[13]

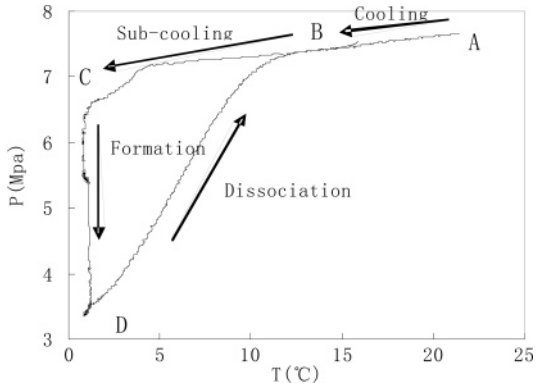

Figure 3. Experimental $P-T$ curve for the hydrate formation/dissociation process.

The inlet pressure profile for a typical run during the hydrate formation process is shown in Figure 4. After the hydrate formation for the first time, it was dissociated in-situ and formed for second or third time. It can be found that the pressure decreases more uniformly with time during the second stage formation than the first one, which suggests that the hydrate formed in the second stage is more uniform in the pressure vessel. The hydrate formation time is greatly shortened during the second stage formation process. For example, the formation time for the first stage formation is around 100 h, while the formation time for the second stage was reduced to less than 35 h. This could be due to the memory effect.[14] A third stage formation has been tried, and no obvious variation in the pressure curve and formation time can be observed, as shown

(13) Sung, W.; Lee, H.; Kim, S. *Energy Sources* **2003**, *25*, 845−856.

(14) Ohgaki, K.; Sugahara, T.; Nakano, S. *J. Chem. Eng. Jpn.* **1999**, *32*, 235−236.

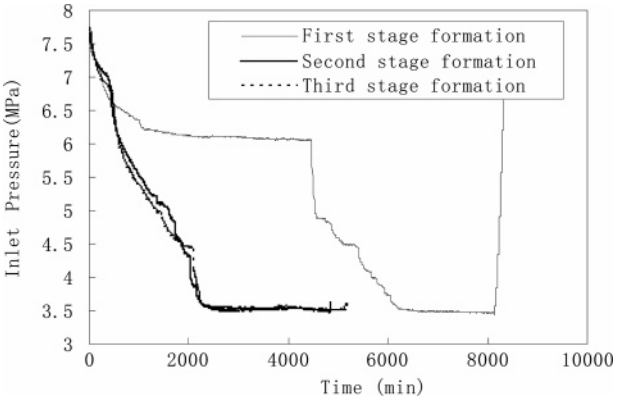

Figure 4. Pressure profile during the hydrate formation process.

in Figure 4. So, a two-stage formation process was chosen for all experimental runs.

2. Depressurization Results. Three depressurization modes have been tested. The first depressurization scheme is accomplished by decreasing the outlet pressure to that of the atmosphere, and the second scheme is to decrease the pressure to 0.93 MPa and then keep the pressure constant. The third one is to decrease the pressure to 1.94 MPa and then keep it constant.

During the depressurization process, the inlet pressure decreases simultaneously with the outlet pressure (back pressure regulator setting value), and the pressure profile is not given here. If the amount of dissociated gas is greater than the amount of gas that can flow out of the core, there would be a pressure increase in the vessel. However, this kind of phenomena has not been observed in all the experimental runs, which suggests that the flow ability of the hydrate core is greater than the hydrate dissociation ability.

The accumulated gas produced from the above three runs is shown in Figure 5a−c. Due to the free gas release from the vessel when the outlet valve was opened, there is a sharp increase of the gas production rate in a very short time at the initial stage for all runs. After that, the gas production rate stays constant, which is due to both the free gas release and hydrate dissociation. In the later stage, the gas production rate begins to slow down until there is no gas released.

The depressurization mode has a great effect on the gas production rate. Run 1, with the pressure decreasing to 0.1 MPa, dissociated much faster than the other two runs. The total dissociation process for run 1 lasted only 15 min, while runs 2 and 3 lasted 40 and 110 min, respectively.

Table 2. Parameters Used for Simulation

	run 1	run 2	run 3	Yousif[6]
number of blocks	100	100	100	50
length of the model (cm)	50	50	50	15
cross-sectional area (cm^2)	11.4	11.4	11.4	11.4
absolute permeability (mdarcy)	300	300	300	100
initial temp (°C)	1.16	1.54	2.08	0.85
initial pressure (MPa)	3.663	3.535	3.584	3.17
porosity (%)	30.8	30.8	30.8	18.8
initial water saturation (%)	29.62	29.61	19.25	17.0
initial hydrate saturation (%)	20.93	21.83	25.44	42.76
P_0 (MPa)	0.1	0.93	1.94	2.495
$\Delta E/R$ (K)	9400	9400	9400	9400
K_0[a] (mol m^{-2} Pa^{-1} s^{-1})	2.1×10^4	1.7×10^4	1.4×10^4	2.3×10^4

[a] Fitted value.

3. Derivation of the Intrinsic Hydration Dissociation Constant. The hydrate simulator TOUGH-Fx/Hydrate has been used to simulate the measured experimental data. The parameters used for the simulation are given in Table 2.

During all the simulations, the hydrate core was regarded as one dimension and was discretized as 100 grids. A schematic

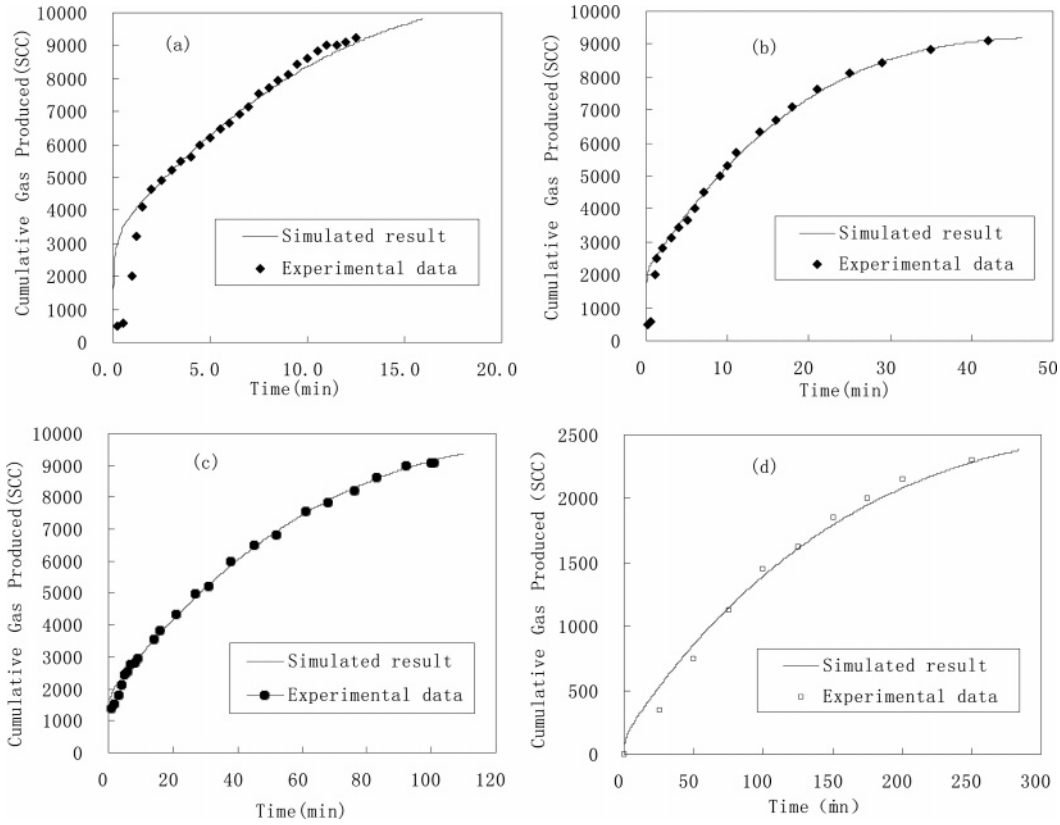

Figure 5. Experimental and simulated cumulative gas produced for experimental runs. (a) Run 1. (b) Run 2. (c) Run 3. (d) Yousif's data.

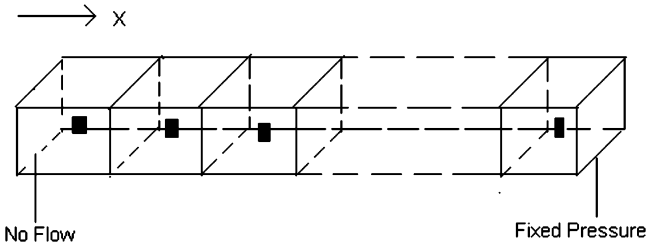

Figure 6. Simulation grid for the experimental hydrate core.

Table 3. Kinetic Parameters

parameters	Kim[12]
$\Delta E/R$ (K)	9400
K_0 (mol m^{-2} Pa^{-1} s^{-1})	1.24×10^5

grid is plotted in Figure 6. The left boundary condition was taken as no flux, while the right boundary condition was taken as the Dirichlet condition (fixed pressure). The temperature boundary condition for both sides was taken as the Neumann condition.

The amount of the initial water and hydrate saturation are calculated by the volume of injected gas and water and gas left after hydrate formation, assuming the hydration number is 6.0. The model for intrinsic permeability reduction due to hydrate formation was chosen as follows:

$$\frac{k}{k_0} = \left(\frac{\phi - \phi_c}{\phi_0 - \phi_c}\right)^n \quad (1)$$

The relative permeability model variation due to hydrate formation is chosen as the Corey model.[10] The intrinsic hydration dissociation constant (K_0) used to describe the hydrate dissociation kinetics in eq 2 was fitted from the experimental cumulative gas produced.

$$Q_g = -K_0 \exp\left(\frac{-\Delta E}{RT}\right) A_s (f_{eq} - f_v) \quad (2)$$

Yousif[6] has done similar experimental work, and his data has also been used in this work.

The fitted K_0 for all the simulations is given in Table 2. The comparison between the experimental and simulated cumulative gas produced is shown in Figure 5. The simulated cumulative gas produced agrees well with the experimental data except at the initial stage. This is because the quick depressurization mode causes the gas release rate to exceed the measurement range (2000 SCC/min) of the flow meter at the initial stage. Hence, the experimental data is difficult to determine at this stage.

The K_0 obtained from the simulation for both our experimental data and Yousif's data is on the order of 10^4 mol m^{-2} Pa^{-1} s^{-1}. Compared with the kinetic parameters for a bulk hydrate dissociation system given by Kim,[12] as shown in Table 3, the K_0 for hydrate dissociation in porous media derived in this work is one order lower. This is because the substantial heat and mass transfer resistance play an important role in hydrate dissociation in porous media.

In a similar work, Yousif[6] reported that the hydrate dissociation rate constant K_d, taken as $K_0 \exp(-\Delta E/RT)$, was on the order of 10^{-13} mol m^{-2} Pa^{-1} s^{-1}. At a temperature in the experimental range, the $\exp(-\Delta E/RT)$ was calculated to be on the order of 10^{-15}, resulting in a K_0 value on the order of 10^2 mol m^{-2} Pa^{-1} s^{-1}, which is two orders of magnitude lower than that of this work reported in Table 2. The two orders underestimation of the K_0 from Yousif's work was possibly due to his overestimation of the reaction surface area (A_s), which is

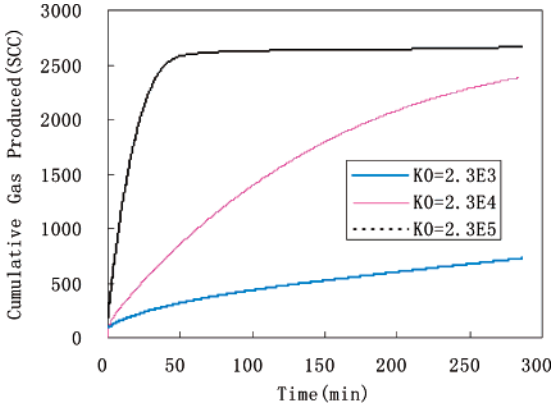

Figure 7. Effect of the K_0 on the gas production behavior for the experimental-scale hydrate core.

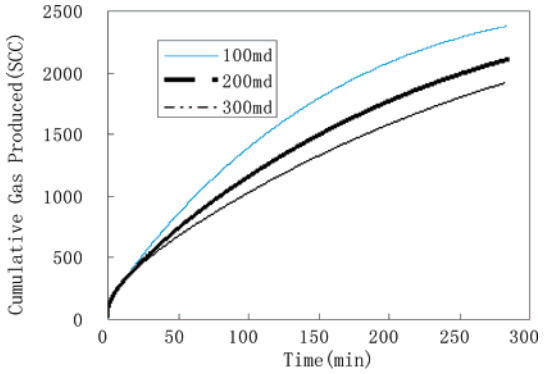

Figure 8. Effect of the permeability on the gas production behavior for the experimental-scale hydrate core.

a parameter hard to measure in porous media and dependent on the pore size and hydrate distribution. The reaction surface area from Yousif's work[6] was calculated as $A_s = \{[(1 - S_H)\varphi]^3/2k\}^{0.5}$, and the calculated value for his experimental hydrate core was on the order of 10^5 m^2, which seems impractical for porous media. The reaction surface area in the simulator,[10] calculated as $A_s = [(1 - \phi)/(4/3)\pi r_p^3)](4\pi r_p^2)(S_H)^{2/3}$, was on the order of 10^3 m^2, which was close to the specific surface area of the porous media used in this work measured by CO_2 adoption. This also suggests that the derived parameter should be cautiously applied to other sediments, such as silt and clay, which have different pore structures than sand.

4. Sensitivity Analysis of the Dissociation Process. In order to determine the controlling mechanism for hydrate dissociation in porous media, a sensitivity analysis based on the TOUGH-Fx/Hydrate has been carried out.

The effect of K_0 on the gas production behavior in Yousif's laboratory-scale hydrate core is given in Figure 7. The result indicated that the intrinsic hydration dissociation constant has a great effect on the gas production behavior. The hydrate dissociation process finishes in much a shorter time if the K_0 was increased by one order; however, decreasing the K_0 value by one order results in an obvious slow gas production process.

By varying the absolute permeability, the effect of the fluid flow ability on the gas production behavior for the laboratory-scale hydrate core has also been investigated, as shown in Figure 8. The effects of absolute permeability on the gas production behaviors seem negligible. Accordingly, the conclusion can be made that the hydrate dissociation process is kinetic-controlled for a laboratory-scale hydrate core.

In addition, an artificial field-scale hydrate reservoir has also been simulated. It has a dimension with a length of 100 m and

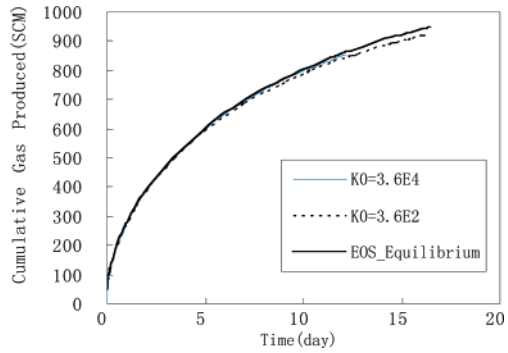

Figure 9. Effect of the K_0 on the gas production behavior for a field-scale hydrate reservoir (standard cubic meter (SCM)).

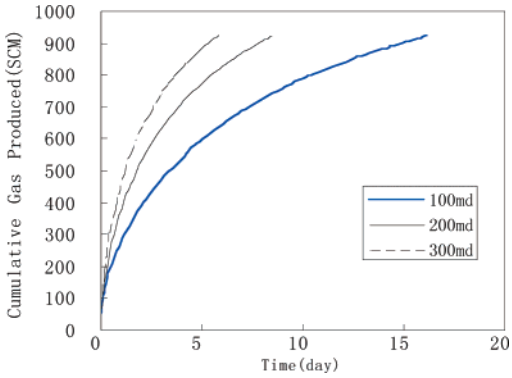

Figure 10. Effect of the permeability on the gas production behavior for a field-scale hydrate reservoir.

a cross-sectional area of 1 m^2, and it has been discretized as 200 grids. Other physical properties and boundary conditions were taken as same as those for the laboratory hydrate core.

The effect of the intrinsic kinetic constant on the gas production behavior for the artificial field-scale hydrate reservoir is shown in Figure 9. The calculated cumulative gas produced obtained from the equilibrium model (EOS_ Equilibrium) in the TOUGH-Fx/Hydrate is also given in this figure. The equilibrium model is used to model the instantaneous hydrate dissociation process, i.e., the hydrate dissociation rate is limitlessly fast when the hydrate equilibrium condition is met. The result clearly indicates that hydrate dissociation kinetics has almost no effect on the gas production behavior for a field-scale hydrate reservoir.

However, the effect of the absolute permeability on the gas production behavior for the field-scale hydrate reservoir is significant, as given in Figure 10. A lower permeability results in a significantly slow gas production rate. Hence, for a field-scale hydrate reservoir, the gas production process is flow-controlled.

In order to determine the different mechanisms for different scale reservoirs, two parameters are defined:

the dissociated gas in unit time:

$$M_D = \int_V K_0 \exp\left(\frac{-\Delta E}{RT}\right) A(f_{eq} - f_v)\, dV \quad (3)$$

the gas flow out of the medium in unit time:

$$M_F = \int_A \nabla(\rho_g v_g)\, dA \quad (4)$$

The ratio between M_D and M_F in a hydrate reservoir can be used as a qualitative indictor of the relative importance of the flow and dissociation mechanisms. In a system, if the dissociated gas in unit time is greater than the flowed gas ($M_D/M_F > 1$),

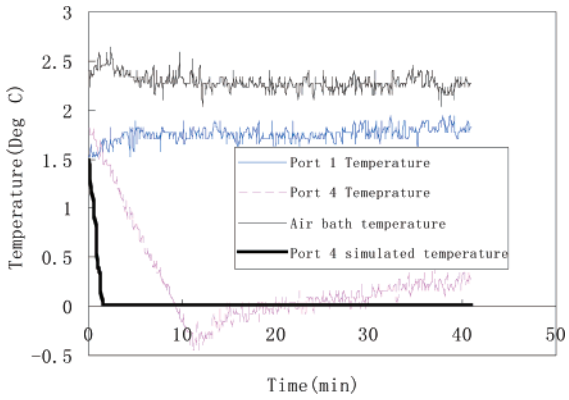

Figure 11. Temperature profile during the gas production process.

Table 4. Controlling Mechanism for Different Scale Hydrate Reservoirs

	run 1	run 2	run 3	Yousif	field
estimated M_{DMax}/M_{FMax}	2.71×10^{-3}	2.04×10^{-3}	2.49×10^{-3}	8.55×10^{-2}	1.4×10^{1}
controlling mechanism	kinetic	kinetic	kinetic	kinetic	flow

the control mechanism is then flow-controlled, otherwise it is kinetic-controlled. The ratio is a function with time during the gas production process and is dependent on of the geometry of the reservoir, depressurization mode, hydrate dissociation kinetics, etc.

In order to estimate the M_D/M_F ratio for the laboratory- and field-scale hydrate reservoirs, the maximum dissociated gas in unit time can be estimated at the maximum dissociation surface area and the largest dissociation drive force, i.e.

$$M_{DMax} = K_0 \exp\left(\frac{-\Delta E}{RT}\right) A_{max}(f_{eq} - f_0)V \quad (5)$$

and the maximum gas flow out of the media in unit time can be estimated at the maximum permeability and the largest flow driving force, i.e.

$$M_{FMax} = \rho_g \frac{K_{max} K_{rg}}{u_g} \frac{P - P_0}{L} \phi A \quad (6)$$

Table 4 gives the estimated ratio between M_{DMax} and M_{FMax} for different kinds of hydrate reservoirs. The ratios are less than 1 for the laboratory-scale hydrate core. Accordingly, it is kinetic-controlled, while the ratio is greater than 1 for a field-scale hydrate reservoir, suggesting that it is flow-controlled. The result agrees with the conclusion from sensitivity analysis.

5. Temperature Profile During the Depressurization Process. The temperature profile during the gas production process for a typical run is given in Figure 11. The result suggests that the outlet temperature decreases sharply when the depressurization process begins and then begins to increase with time at a later stage. The temperature decrease may becuase of the following two reasons: (1) The hydrate dissociation is an endothermic process; (2) The gas expands when released to a low-pressure environment, resulting in the decrease of temperature. The inlet temperature, however, stays constant due to the heat being easily transfered into the steel vessel.

The simulated temperature profile from the hydrate simulator does not agree well with the experimental temperature profile, and the simulated temperature profile decreases much more quickly than the experimental profile, as given in Figure 11. The temperature deviation could be attributed to the following factors: (1) The mode of the simulation has some defects, as

the domain description did not include the steel vessel, which plays an important role in the heat transfer process during the gas production process; (2) There is no accurate thermal property data for all the materials involved in the experiment, and there is no proper model in modeling the heat transfer between the environment and the steel vessel; (3) The throttle effect of the water and gas release from the valve contributes; (4) The issue of the accuracy of the temperature measurement (inertia in the response) can also contribute to the deviation between measured and simulated value. For these reasons, such temperature deviations are then fully expected. The author then has assumed that the temperature distribution in all the previous simulations had no effect on the simulated intrinsic kinetic dissociation constant.

Conclusions

Methane gas production behavior from an experimental-scale hydrate reservoir by depressurization has been studied. A hydrate reservoir simulator TOUGH-Fx/Hydrate has been used to predict the experimental results. The following conclusions can be made:

(1) The TOUGH-Fx/Hydrate simulator can be successfully applied for the simulation of the gas hydrate production behavior of a laboratory-scale hydrate core

(2) The intrinsic hydration dissociation constant for all the experimental runs fitted from the simulator is on the order of 10^4 mol m^{-2} Pa^{-1} s^{-1}, which is one order lower than the value from bulk hydrate dissociation.

(3) Different mechanisms control the hydrate dissociation process for laboratory- and field-scale hydrate reservoirs. Hydrate dissociation kinetics is important for the production process of a laboratory-scale hydrate core. However, for a field-scale hydrate reservoir, the flow mechanism dominates the production process and hydrate dissociation kinetics has almost no effect on the gas production behavior.

Acknowledgment. The financial supports from the Natural Sciences Foundation (No. 06301036) of Guangdong Province and the Research Program of the One-Hundred Talent Project of the Chinese Academy of Sciences are gratefully acknowledged. The granting of a license for TOUGH Fx/Hydrate version 1.0 from the Berkeley National Laboratory and suggestions from Dr. G. J. Moridis in using the software are also acknowledged.

Nomenclature

A = reservoir cross-sectional area (m^2)
A_0 = theinitial surface area (m^2)
A_s = thesurface area participating in the dissociation (m^2)
ΔE = thehydration dissociation activation energy (J mol^{-1})
f_{eq} and f_v = fugacity at equilibrium and in the gas phase at temperature T (Pa)
k = reservoir absolute permeability (mdarcy)
k_{rg} = gas relative permeability
K_0 = theintrinsic hydration dissociation constant (mol m^{-2} Pa^{-1} s^{-1})
K_d = thehydrate dissociation rate constant (mol m^{-2} Pa^{-1} s^{-1})
L = thelength of the reservoir (m)
n = permeability reduction coefficient
P = hydrate reservoir pressure (Pa)
P_0 = theoutlet pressure (Pa)
R = theuniversal gas constant (8.314 J mol^{-1} K^{-1})
r_p = particle radius (m)
S_H = hydrate saturation
T = thereservoir temperature (K)
V = thehydrate reservoir volume (m^3)
φ = porosity (%)
φ_c = critical porosity at which permeability is reduced to zero (%)
υ_g = gas velocity (m s^{-1})
μ_g = gas viscosity (Pa s)
ρ_g = gas density (kg m^{-3})

EF0601869